



Article

Power Injection and Free Resonance Decoupled Wireless Power Transfer System with Double-Switch

Wei Wu ¹, Daqing Luo ^{2,*}, Zhe Tang ², Jianfeng Hong ³ and Junjie Yang ²

¹ School of Mechanical & Electrical Engineering, Guizhou Normal University, Guiyang 550025, China; wuwei233@hotmail.com

² Department of Instrumental and Electrical Engineering, Xiamen University, Xiamen 361005, China; 35120211151591@stu.xmu.edu.cn (Z.T.); 19920130154226@stu.xmu.edu.cn (J.Y.)

³ School of Mechanical and Automotive Engineering, Xiamen University of Technology, Xiamen 361005, China; hjf156@sina.com

* Correspondence: daqingluo_del@163.com; Tel.: +86-186-9505-0050

Abstract: This article presents a type of power injection and free resonance decoupled wireless power transfer (WPT) system, the double-switch independent power injection and free resonance wireless power transfer (IPIFR-WPT) system working in CCM. Based on the stroboscopic mapping model, the theoretical results show that the operation point of the proposed WPT system is determined by itself instead of the switching control strategy. Specifically, once the voltage on the primary capacitance does not decrease to the input voltage in the free-resonance process, the diode in series would not turn on and the system would not switch to the power injection process. Therefore, there is a wide soft-switching margin to ensure the system operating in soft-switching states. Another characteristic of the proposed WPT system is the monotonicity between output power and operation cycle, which presents a simple power control method. And since the soft-switching margin may have intersection under dynamic coupling coefficient, the proposed system maintains soft-switching states with a fixed switching strategy and presents advantage to resist the dynamic change of coupling coefficient. All the characteristics of the proposed WPT system mentioned above have been verified in both theory and experiment.

Keywords: decouple; wireless power transfer; power injection; soft switching; power control



Citation: Wu, W.; Luo, D.; Tang, Z.; Hong, J.; Yang, J. Power Injection and Free Resonance Decoupled Wireless Power Transfer System with Double-Switch. *Electronics* **2023**, *12*, 4061. <https://doi.org/10.3390/electronics12194061>

Academic Editors: Alon Kuperman, Deniss Stepins and Janis Zakis

Received: 14 August 2023

Revised: 19 September 2023

Accepted: 25 September 2023

Published: 27 September 2023



Copyright: © 2023 by the authors. Licensee MDPI, Basel, Switzerland. This article is an open access article distributed under the terms and conditions of the Creative Commons Attribution (CC BY) license (<https://creativecommons.org/licenses/by/4.0/>).

1. Introduction

The wireless power transfer (WPT) system is mainly based on the principle of electromagnetic induction and high-frequency inverter technology to transfer power wirelessly from a primary coil to one or more moveable secondary coils across air gaps [1]. There is no direct physical connection between the primary coil and secondary coil and they are coupled by electromagnetic fields. Hence, WPT technology is an ideal solution for connector-free, moveable or rotatable devices, especially electric vehicles, robots, portable devices and even underwater devices [2–6].

Usually, WPT systems including LC, LCL and LCC systems using a variety of compensation networks are fully resonant types, that is, all working modes of the systems are in resonant state [7–11]. Power injection and system resonance are completed simultaneously. The fully resonant type WPT system works well under static operation condition. However, since the primary and secondary coils are not rigidly connected, the coil dynamic offset and vibration could be caused by environmental impact. By changing the system coupling coefficient and load resistance during operation, the impedance of the fully resonant type WPT system will change and the output power and operation efficiency will be greatly reduced. In order to ensure fully resonant type WPT systems work at the maximum power operation point or the maximum efficiency operation point under dynamic parameters, some closed-loop methods have been proposed, such as the impedance compensation

methods and the frequency tracking methods [12,13]. However, the required operation points of the fully resonant type WPT system may exist in non-unique solutions, which brings difficulty for these closed-loop methods [14–16].

The independent power injection and free resonance wireless power transfer (IPIFR-WPT) system has been proposed, whose processes of power injection and resonance are decoupled instead of happening at the same time like the fully resonant type [17–19]. Article [17] described the performance of an IPIFR-WPT system with six switches working in discontinuous current mode (DCM) and put forward the corresponding equivalent linear models. Similar to the DCM mode of the BUCK circuit, there are three modes in one steady-state period in the six-switch topology, that is, power injection mode, self-resonance mode and stop mode. In the stop mode, the current through the primary-side inductor is zero. Hence, the stop mode has no contribution to transfer power and the power density is not very high. Then, a new IPIFR-WPT system with six switches working in continuous current mode (CCM) was proposed [18]. Similar to the CCM mode of the BUCK circuit, there are two modes in one steady-state period, that is power injection mode and self-resonance mode. Working in CCM, the current through the primary-side inductor is continuous and does not remain zero. However, in both articles [17,18], there was no theoretical method to determine the periods of the linear subsystems.

To simplify the modes and decrease the number of switches, article [19] proposed another type of IPIFR-WPT system with two switches working in DCM and described the easy power control method and the wide range of soft-switching operation. But only an approximate model had been put forward and the calculated result was not totally precise. As the case when the system parameters changed has not been discussed, the wide range of soft-switching operation could not be proved fully.

This article is trying to study the characteristics of self-determining operation point and open-loop adaptability in the double-switch type of IPIFR-WPT system working in CCM. The main work of this article is to present a theoretical method based on the stroboscopic mapping to determine the precise operation point of each linear subsystem when the system achieves a steady state [20]. All the performance can be predicted with the determined precise operation point. Furthermore, the characteristics of the proposed WPT system including the self-determining soft-switching operation point and the monotonicity of power curve about the cycle can all be verified.

In Table 1, the comparison between the proposed system and the similar systems has been listed. In the CCM operation mode, the proposed system has only four control modes, which means its control strategy is simpler than the other topologies.

Table 1. The comparison between the proposed system and similar systems.

Reference	Number of Switches	Operation Mode	Maximum Efficiency (%)	Number of Control Modes
[17]	6	DCM	93.6	10
[18]	6	CCM	89.6	10
[19]	2	DCM	88.4	6
the proposed system	2	CCM	91.6	4

Note that the power injection process and the free-resonance process of the IPIFR-WPT system are independent. The self-determining soft-switching operation point means that the IPIFR-WPT system can automatically adjust the real intervals of each process under both the static and dynamic system parameters, which allows the switching strategy that has a wide soft-switching margin to let the control process be flexible. And the monotonicity of power curve about cycle means that the input and output power of the proposed WPT system can be controlled continuously instead of being limited by the power peak, which could simplify the power control method.

2. Mode Analysis and Operation Point Calculating Method

2.1. Mode Analysis

The main circuit diagram of the IPIFR-WPT system is shown in Figure 1. The diode D_0 is used to prevent current backflow. The switch S_1 is used to connect the dc voltage source E_{dc} to the circuit of the primary side. Besides, there is a switch S_2 control to access the resonant capacitor C_p on the primary side. The primary self-inductance L_p with internal resistance R_p and the secondary self-inductance L_s with internal resistance R_s constitute the mutual inductance coil, the main power transfer element. Additionally, between the primary coil and the secondary coil, M is the mutual inductance and k is the coupling coefficient. C_s is the filter capacitor on the secondary side. In addition, a rectifier bridge in parallel with a relatively large capacitor C_0 in the secondary side to filter a dc output, and the real load R and the equivalent load R_L have the following relationship [21]:

$$R_L = \frac{8R_0}{\pi^2} \tag{1}$$

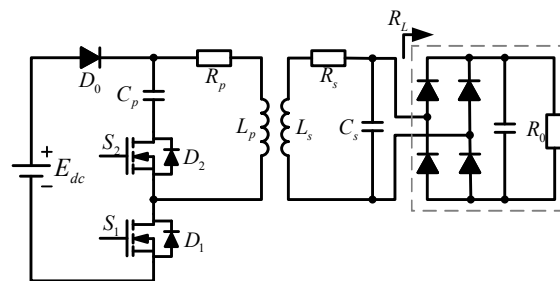


Figure 1. The double-switch IPIFR-WPT system.

The operation modes of the proposed system in CCM are shown in Figure 2. On Figure 2, u_p , i_p , i_s and u_o are the state variables on C_p , L_p , L_s and C_s , respectively. And i_1 is the current across the diode D_0 . The power injection process only includes Mode 1, shown in Figure 2a. The self-resonance process consists of Mode 2, Mode 3 and Mode 4, which are shown in Figure 2b–d, respectively. Since the performance on the primary side matters the stability of converter directly, only the operation curves of i_p and u_p are shown in Figure 3. The operation time of power injection process and self-resonance process are ζ_1 and ζ_2 , respectively.

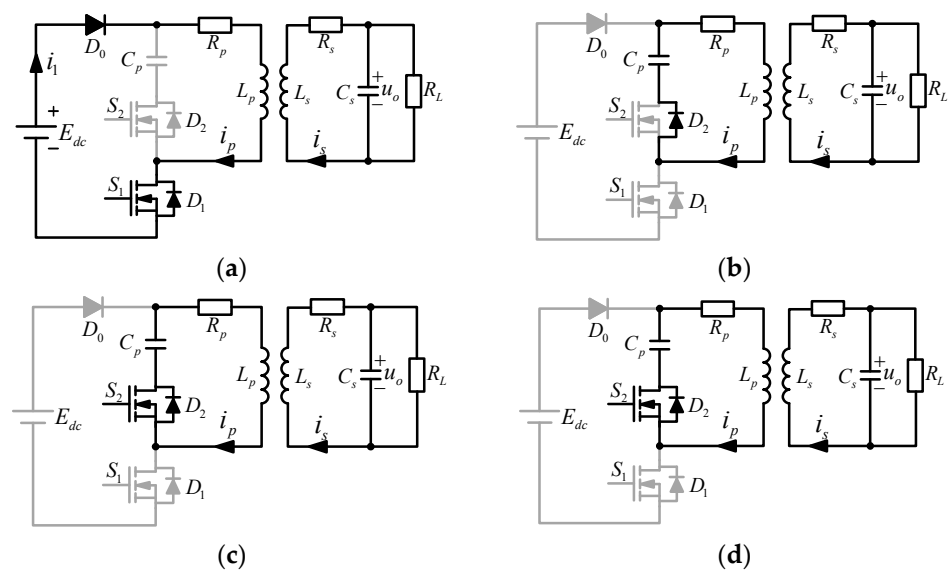


Figure 2. The double-switch IPIFR-WPT system. (a) Mode 1, (b) Mode 2, (c) Mode 3, (d) Mode 4.

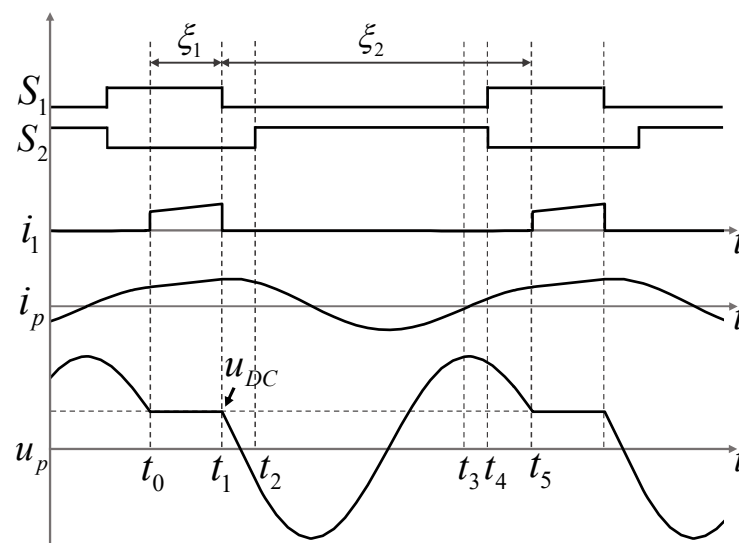


Figure 3. The operation curves of the double-switch IPIFR-WPT system working in CCM mode.

Mode 1 $[t_0, t_1]$: Mode 1 is the power injection process, which is shown as Figure 2a. Before t_0 , the switch S_1 has been already turned on and the switch S_2 has been turned off. But before t_0 , $u_p > E_{dc}$ and the diode D_0 was not conducting, meanwhile the current i_p flowed through the bypass diode D_2 . At the time t_0 , u_p decreases to E_{dc} and the diode D_0 is conducting so that the current i_p is commutated from the bypass diode D_2 to S_1 . Meanwhile, C_p will be isolated from the system and the dc supply E_{dc} will charge the inductor L_p directly. The primary current i_p across L_p is unidirectional to ensure the turning-on of the diode D_0 , namely, $i_p > 0$. Note that in mode 1, $i_1 = i_p$.

Mode 2 $[t_1, t_2]$: Mode 2 in Figure 2b is an incomplete self-resonance process. At t_1 , the switch S_1 turns off and the switch S_2 remains off, but the current $i_p > 0$ so that the current i_p is commutated from the switch S_1 to the bypass diode D_2 naturally, meanwhile $i_1 = 0$. Since the operation time of Mode 2 is very short, the current i_p will satisfy that $i_p > 0$ during Mode 2.

Mode 3 $[t_2, t_4]$: Mode 3 in Figure 2c is a complete self-resonance process. At the time t_2 , the switch S_2 turns on to let the capacitor C_p and the inductor L_p connect to each other to form a resonant network. Since $i_p > 0$, the diode D_0 is conducting. If the tube voltage drop of D_2 is ignored, the turning-on process of S_2 meets the opening zero voltage switching (ZVS) condition.

Mode 4 $[t_4, t_5]$: Mode 4 in Figure 2d is an incomplete self-resonance process. At the time t_4 , the switch S_1 turns on meanwhile S_2 turns off. Since $i_p > 0$, the current i_p remains conducting in the diode D_2 to let the turning-off of S_2 meet the ZVS condition. Meanwhile as $u_p > E_{dc}$, the diode D_2 is not conducting so that no current flows through the switch S_1 . Hence, the turning-on of S_1 meets the zero current switching (ZCS) condition. And the current i_p will not be commutated from the diode D_2 to the switch S_1 until the time t_5 where $u_p = E_{dc}$.

2.2. Calculating Method of the Operation Point

In the IPIFR-WPT system working in the CCM mode, the processes can be divided into two independent subsystems including the power injection Σ_1 and the self-resonance Σ_2 , whose equivalent circuits are shown in Figure 4.

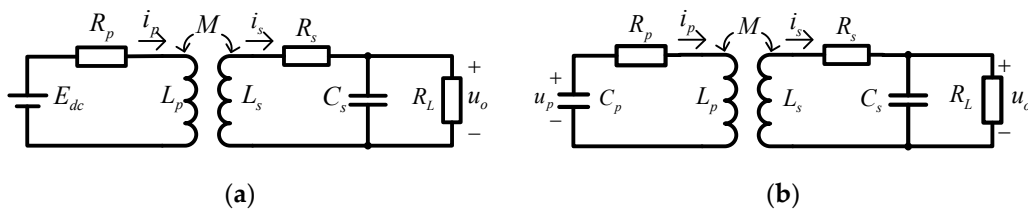


Figure 4. The equivalent circuits of double-switch IPIFR-WPT system. (a) The power injection process Σ_1 . (b) The self-resonance process Σ_2 .

During the power injection process, which is shown in Figure 4a, the capacitor C_p is isolated from the system and the dc supply E_{dc} is connected to the system. The power is injected to the system, meanwhile up remains satisfying $u_p = E_{dc}$ during the power injection process.

During the self-resonance process, which is shown in Figure 4b, E_{dc} is isolated from the system while L_p and C_p are connected to each other to form a resonant network. As a result, the power will transfer from the primary side to the secondary side during the self-resonance process.

Let $x = [u_p, i_p, i_s, u_o]^T$ and $u = [E_{dc}]$ be the state vector and the input vector of the system, respectively. And the reference directions of every state have marked been on Figure 4. According to the Kirchoff’s voltage and current laws, the equivalent circuit shown in Figure 4a of the two subsystems Σ_1 and Σ_2 can be described by the differential equations as follows:

Σ_1 : the equation for power injection is

$$\dot{x} = A_1x + B_1u \tag{2}$$

Σ_2 : the equation for self-resonance is

$$\dot{x} = A_2x \tag{3}$$

where:

$$A_1 = \begin{bmatrix} 0 & 0 & 0 & 0 \\ 0 & \frac{L_s R_p}{\Delta} & \frac{M R_s}{\Delta} & \frac{M}{\Delta} \\ 0 & \frac{M R_p}{\Delta} & \frac{L_p R_s}{\Delta} & \frac{L_p}{\Delta} \\ 0 & 0 & \frac{1}{C_s} & -\frac{1}{C_s R_L} \end{bmatrix}$$

$$B_1 = \begin{bmatrix} 0 & \frac{-L_s}{\Delta} & \frac{-M}{\Delta} & 0 \end{bmatrix}^T$$

$$A_2 = \begin{bmatrix} 0 & -\frac{1}{C_s} & 0 & 0 \\ \frac{-L_s}{\Delta} & \frac{L_s R_p}{\Delta} & \frac{M R_s}{\Delta} & \frac{M}{\Delta} \\ \frac{-M}{\Delta} & \frac{M R_p}{\Delta} & \frac{L_p R_s}{\Delta} & \frac{L_p}{\Delta} \\ 0 & 0 & \frac{1}{C_s} & -\frac{1}{C_s R_L} \end{bmatrix}$$

$$\Delta = M^2 - L_p L_s$$

$$M = k\sqrt{L_p L_s}$$

The solution of linear system Σ_1 and Σ_2 can be expressed as follows:
 Σ_1 : the equation for power injection is

$$x(t) = \Phi_1(t)x_0 + \int_{t_0}^{t+t_0} \Phi(t_0 + t - \tau)B_1E_{dc}d\tau \tag{4}$$

Σ_2 : the equation for self-resonance is

$$x(t) = \Phi_2(t)x_0 \tag{5}$$

where $x_0 = x(t)|_{t=0}$, $\Phi_1(t) = \exp\{A_1t\}$ and $\Phi_2(t) = \exp\{A_2t\}$.

Note that the integral term in (4) is a zero-input response, whose value is a single valued function about time. Let $Y_{zi}(t)$ replace this integral term to simplify writing and Equation (4) can be rewritten as follows:

$$x(t) = \Phi_1(t)x_0 + Y_{zi}(t) \tag{6}$$

The iterative relationship of the IPIFR-WPT system in n th operation cycle is shown in Figure 5. The intervals of subsystems Σ_1 and Σ_2 are ξ_1 and ξ_2 , respectively. x_n is the initial state variables. After the time spans ζ_1 and ζ_2 of the two subsystems, an intermediate state variable x_{n1} and the terminal state variable x_{n+1} can be described as follows:

$$x_{n1} = \Phi_1(\zeta_1)x_n + Y_{zi}(\zeta_1) \tag{7}$$

$$x_{n+1} = \Phi_2(\zeta_2)\Phi_1(\zeta_1)x_n + \Phi_2(\zeta_2)Y_{zi}(\zeta_1) \tag{8}$$

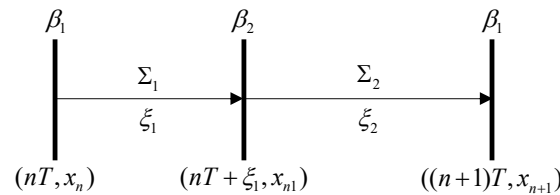


Figure 5. The iterative relationship of double-switch IPIFR-WPT system in n th operation cycle.

Once the system operates in steady state, the state variables must be periodic, namely, $x_{n+1} = x_n$. Equation (8) is a mapping from x_n to x_{n+1} , therefore $x^* = x_n = x_{n+1}$ can be described as a fixed point in this mapping, whose equation is presented as follows:

$$x^* = [I - \Phi_2(\zeta_2)\Phi_1(\zeta_1)]^{-1}\Phi_2(\zeta_2)Y_{zi}(\zeta_1) \tag{9}$$

Let the operation cycle T be a constant and bring $\zeta_2 = T - \zeta_1$ in (9), then the equation can be rewritten as follows:

$$x^* = [I - \Phi_2(T - \zeta_1)\Phi_1(\zeta_1)]^{-1}\Phi_2(T - \zeta_1)Y_{zi}(\zeta_1) \tag{10}$$

Based on the mode analysis, the boundary β_1 and β_2 shown in Figure 5 can be described as follows:

When Σ_2 switches to Σ_1 , the boundary is β_1 : $u_p = E_{dc}$ & $i_p > 0$,

When Σ_1 switches to Σ_2 , the boundary is β_2 : $S_1 = 0$.

The boundary β_1 is determined by the value of state variables instead of the actions of switches. Concretely, before the boundary β_1 , the system works in the free-resonance process, since the voltage u_p is greater than E_{dc} , the resonant current i_p flow through the resonant tank consists of C_p and L_p even the switch S_1 has been already turned-on. At the moment of β_1 , the voltage u_p decreases to E_{dc} and the current i_p completes commutation

from D_2 to S_1 . Therefore, the voltage u_p equals to E_{dc} at the boundary β_1 and the equation can be expressed as follows:

$$C_1[I - \Phi_2(T - \zeta_1)\Phi_1(\zeta_1)]^{-1}\Phi_2(T - \zeta_1)Y_{zi}(\zeta_1) = E_{dc} \tag{11}$$

where, $C_1 = [1, 0, 0, 0]$.

Make a new function as follows:

$$f(\zeta_1) = C_1[I - \Phi_2(T - \zeta_1)\Phi_1(\zeta_1)]^{-1}\Phi_2(T - \zeta_1)\frac{Y_{zi}(\zeta_1)}{E_{dc}} - 1 \tag{12}$$

The result of $f(\zeta_1) = 0$ will meet the steady-state condition. The parameters of the IPIFR-WPT system are shown in Table 2 and the operation cycle $T = 100 \mu s$.

Table 2. The -parameters of the double-switch IPIFR-WPT system.

Parameter	E_{dc} (V)	L_p (μH)	C_p (μF)	R_p (Ω)	L_s (μH)
Value	100	660	0.4	0.2	585
Parameter	C_s (μF)	R_s (Ω)	k	R_L (Ω)	
Value	0.4	0.2	0.5	10	

The curves of the function $f(\zeta_1)$ with $T = 100 \mu s$ are shown in Figure 6. There are two results of $f(\zeta_1) = 0$, that is, $\zeta_{1a} = 13.09 \mu s$ and $\zeta_{1b} = 36.71 \mu s$. Then, bring ζ_{1a} and ζ_{1b} into (10) to solve the corresponding fixed point, respectively, and the results are shown in Table 3.

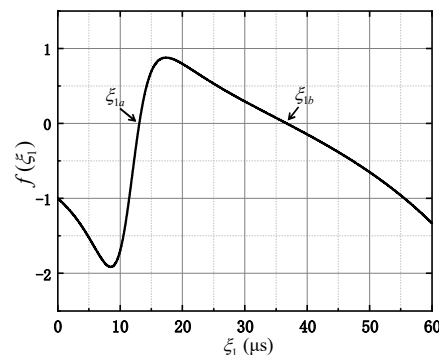


Figure 6. The curves of the function $f(\zeta_1)$.

Table 3. The fixed point of the double-switch IPIFR-WPT system.

ζ_1 (μs)	Fixed Point x^*			
	u_p (V)	i_p (A)	i_s (A)	u_o (V)
13.09	100.0	5.774	3.289	28.72

According to the calculated result of fixed point, for $\zeta_{1a} = 13.09 \mu s$, $u_p = E_{dc}$ and $i_p = 5.774A > 0$ are both satisfied, which means the boundary β_1 is meeting and this result $\zeta_{1a} = 13.09 \mu s$ can be accepted. As for $\zeta_{1b} = 36.71 \mu s$, $u_p = E_{dc}$ is satisfied but $i_p = -2.927A < 0$, which means the boundary β_1 is not meeting and this result will be rejected.

Now, the operation point has been solve out and fixed point has been determined. Furthermore, the continuous solution of state variables in one steady cycle $[nT, (n + 1)T]$ can be presented as follows:

$$x(t) = \begin{cases} \Phi_1(t - nT)x^* + Y_{zi}(t - nT), & t \in [nT, nT + \zeta_1] \\ \Phi_2(t - nT - \zeta_1)x_{n1}^*, & t \in (nT + \zeta_1, (n + 1)T) \end{cases} \tag{13}$$

Bring $\xi_1 = 13.09 \mu\text{s}$ and the corresponding fixed point shown in Table 3 into (13), then the waveforms of $i_p(t)$ and $u_p(t)$ with can be calculated and plotted in Figure 7. Ξ_1 and ξ_2 is the intervals of subsystems Σ_1 and Σ_2 , respectively.

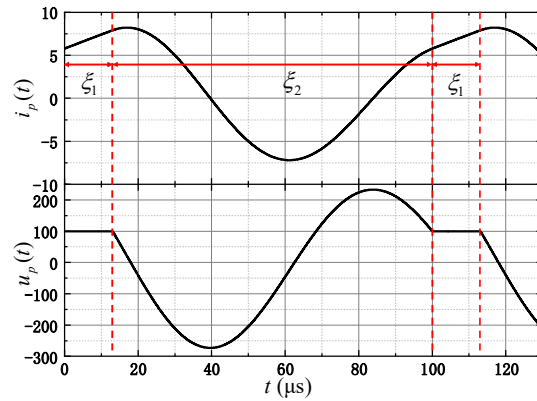


Figure 7. The calculated waveforms of $i_p(t)$ and $u_p(t)$.

3. System Characteristics

3.1. The Wide Soft-Switching Margin Characteristic

The switching condition for Σ_2 switching to Σ_1 , namely, the boundary β_1 , is not determined by the switching actions, which is a remarkable characteristic different from the other WPT system. In the mode analysis shown in Figure 2, S_1 has already been turned-on in Mode 4 and the system mode will not switch to Mode 1 until the voltage u_p decreases to E_{dc} . Hence, the switching strategies are not strictly corresponding to the real operation points. Holding the switching cycle $T = 100 \mu\text{s}$ unchanged, the curves of three switching control methods with different pulse widths, which is the simulation results by Matlab Simulink, are shown in Figure 8.

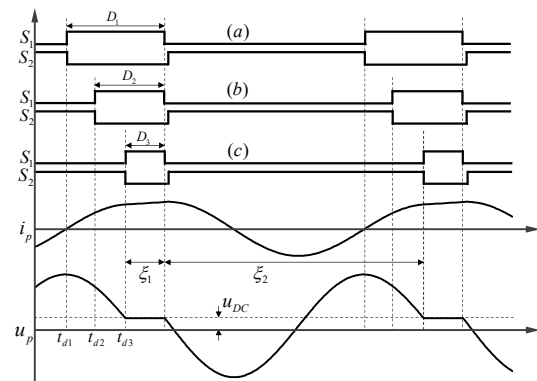


Figure 8. Curves of three switching strategies. (a) $D_1 = 29.07 \mu\text{s}$, (b) $D_2 = 20.00 \mu\text{s}$, (c) $D_3 = 13.09 \mu\text{s}$.

Based on the analysis above, once $u_p > E_{dc}$ and $i_p > 0$ are both satisfied at the moment of turning-on S_1 while turning-off S_2 , the boundary β_1 will meet and the operation point will be self-determined by the system. In Figure 8a, the maximum duty of S_1 has been taken at the critical position of $i_p = 0$. In Figure 8c, the minimum duty of S_1 has been taken at the boundary position of $u_p = E_{dc}$. Hence, once the duty of S_1 takes any values in the margin $[D_3, D_1]$, the operation points of the double-switch IPIFR-WPT system will be self-determined to be the same and the waveforms of $u_p(t)$ and $i_p(t)$ are also the same. And the margin $[D_3, D_1]$ is called the soft-switching margin.

In the case that the system parameters take the value in Table 2 and $T = 100 \mu\text{s}$, the soft-switching margin is $[13.09 \mu\text{s}, 29.07 \mu\text{s}]$, which takes 15.98% of the cycle T . No matter what value in $[13.09 \mu\text{s}, 29.07 \mu\text{s}]$ has been taken as the duty of S_1 , the intervals of power injection

and self-resonance are 13.09 μs and 86.91 μs , respectively, namely, the same operation point has been determined by the system itself instead of the switching strategies. Hence, there is a great margin to ensure the system work is steady and the difficulty of control strategies can be reduced greatly. And note that the value of minimum duty equals to the determined interval ζ_1 of power injection process.

3.2. Self-Determining Soft-Switching Operation Point under Dynamic Coupling Coefficient

Since the switching strategies of the proposed WPT system have a wide soft-switching margin under static system parameters, the soft-switching margin may have overlapping parts under different system parameters. Therefore, the operation point could be self-determined under dynamic system parameters but the same switching strategies. Of all parameters, the coupling coefficient k is the most prone to change dynamically due to the relative movement of the coils.

When k changes from 0.3 to 0.6, the curves of soft-switching margin [D_{min} , D_{max}] can be plotted as Figure 9 and Mar is defined as the percentage of this margin in cycle T as follows:

$$Mar = \frac{D_{max} - D_{min}}{T} \times 100\% \tag{14}$$

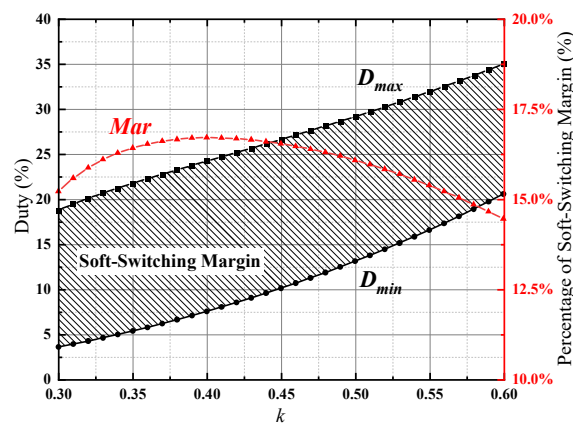


Figure 9. Curves of three switching strategies.

When the switching strategies remain in the shadow part between the curves of D_{min} and D_{max} on Figure 9, the system will keep working in soft-switching operation state under dynamic change of k . And the percentage Mar remains above 14.4%, which indicates that there is a wide soft-switching margin to ensure the system working under dynamic change of k .

According to Figure 9, if we let k equal to 0.45, 0.50 and 0.55, respectively, meanwhile the duty of S_1 remains as 20%, the system will work in a soft-switching margin under the three situations. Namely, when k changes from 0.45 to 0.55 dynamically, the switching strategies keep the same, $T = 100 \mu\text{s}$ and $D = 25\%$.

Then, as shown in Figure 10, the waveforms of $i_1(t)$, $i_p(t)$ and $u_p(t)$ are plotted when k equals to (a) 0.45, (b) 0.50 and (c) 0.55, respectively. The determined intervals ζ_1 by the system itself are (a) 10.09 μs , (b) 13.09 μs and (c) 16.55 μs correspondingly and the boundary conditions β_1 are all meeting in the three figures. Therefore, when the switching strategies remain the same and the coupling coefficient k changes dynamically, the IPIFR-WPT system can keep working in soft-switching states by self-determining its operating point.

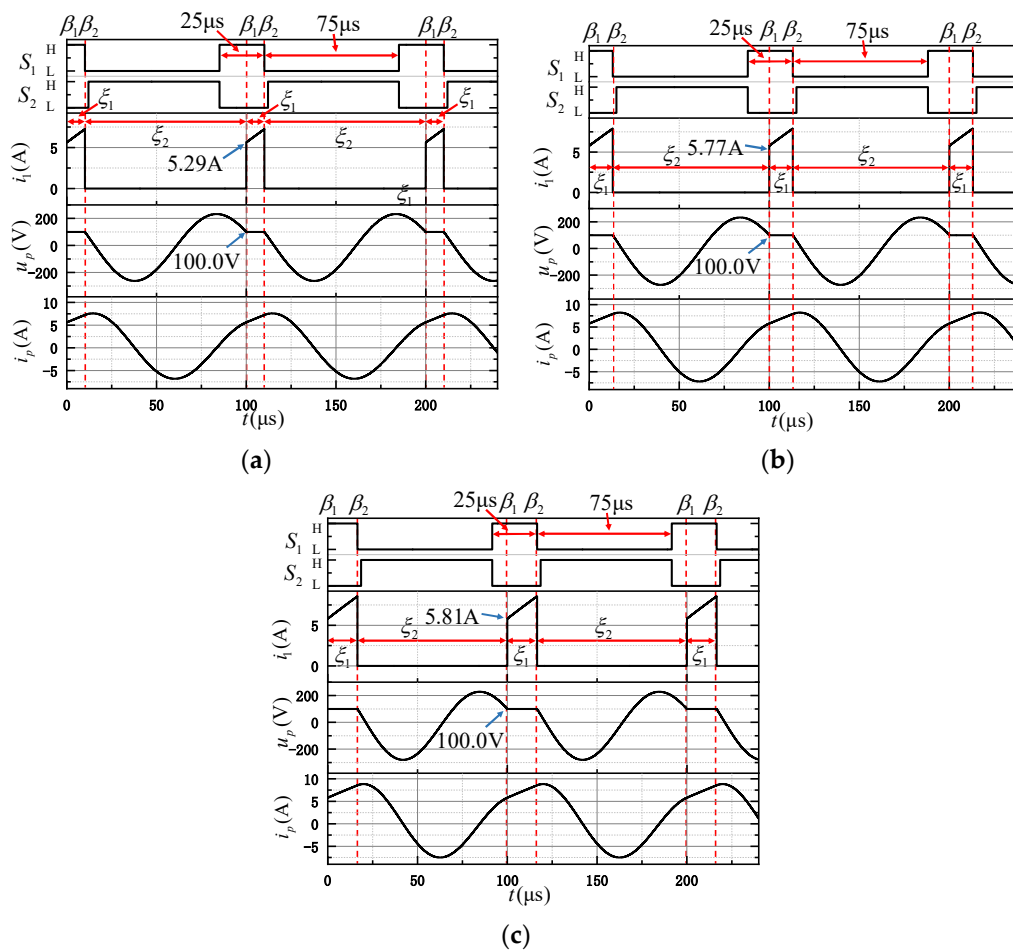


Figure 10. The waveforms of $i_1(t)$, $i_p(t)$ and $u_p(t)$ under different k . (a) $k = 0.45$, (b) $k = 0.50$, (c) $k = 0.55$.

3.3. The Monotonicity of Power about Cycle

Since Equation (13) can solve the time series of the state variables $x(t)$ of the IPIFR-WPT system in one steady-state cycle, it is simple to calculate the input and output power as follows:

$$P_{in} = \frac{E_{dc}}{T} \int_0^{\xi_1} i_p(t) dt \tag{15}$$

$$P_{out} = \frac{1}{TR_L} \int_0^T u_o^2(t) dt \tag{16}$$

$$\eta = \frac{P_{out}}{P_{in}} \times 100\% \tag{17}$$

where $i_p(t) = [0, 1, 0, 0]x(t)$ and $u_o(t) = [0, 0, 0, 1]x(t)$, η is the efficiency of the whole system.

According to the characteristic of a self-determining operation point, it is illustrated that the switching strategies of double-switch IPIFR-WPT system has a wide margin to ensure the soft-switching operation states and the duty of S_1 does not determine the operation point. The operation cycle T can be used to adjust the output power and the relationship of output power P_{out} with cycle T is shown in Figure 11.

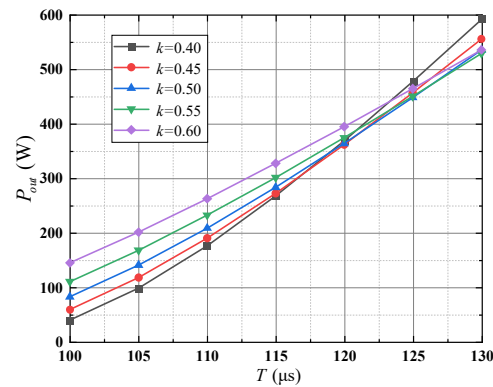


Figure 11. The relationship of output power P_{out} with cycle T .

In Figure 11, there is a monotonic relationship between the output power P_{out} and cycle T and the linear relationship between P_{out} and T becomes more obvious when the coupling coefficients k increase. Hence, it is simple to control the output power by adjusting the cycle T , namely, the frequency f of the IPIFR-WPT system.

In Figure 12, the corresponding efficiency η has been plotted and the efficiency η has few decreases with the increases of cycle T . Therefore, the efficiency η maintains few changes when the system control the output power by adjusting frequency.

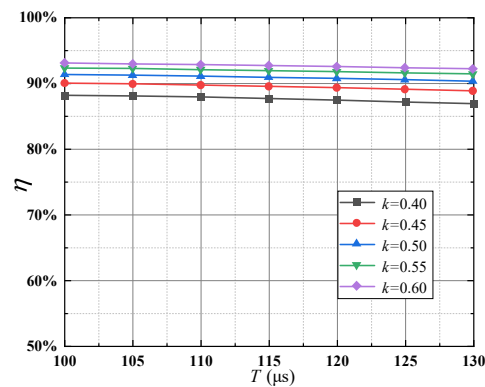


Figure 12. The relationship of efficiency η with cycle T .

4. Experimental Verification

4.1. Experimental Devices

Based on the main circuit of the double-switch IPIFR-WPT system, the experimental system has been built as shown in Figure 13a. The part of the DC voltage source consists of the AC voltage regulator and rectifier module (MDQ100A1600V). As shown in Figure 13b, the converter is composed of the MOSFET driver (SI8233), the MOSFET (C2M0045120D), the diode D_0 (MURF2060) and the microcontroller (STM32F107VC). The values of L_p , C_p , L_s , C_s and R_L are selected as Table 2. And the oscilloscope and power analyzer are RTB2004 (Ronde & Schwarz, Munich, Germany) and WT500 (Yokogawa, Musashino, Japan), respectively.

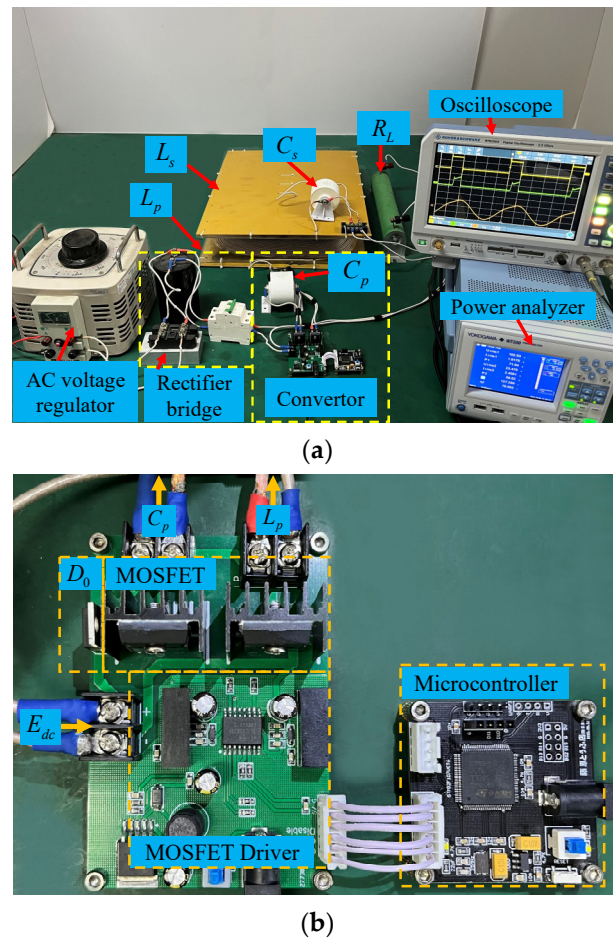


Figure 13. Experiment devices. (a) Experimental System. (b) MOSFET converter.

The relationship between the coupling coefficient k and the distance d of the coils are shown in Figure 14. With the increases of the distance d from 5 cm to 20 cm, the coupling coefficient k decreases from 0.64 to 0.12. Notice, in the follow-up experiments, the coupling coefficient k is always changed via changing the distance of the coils.

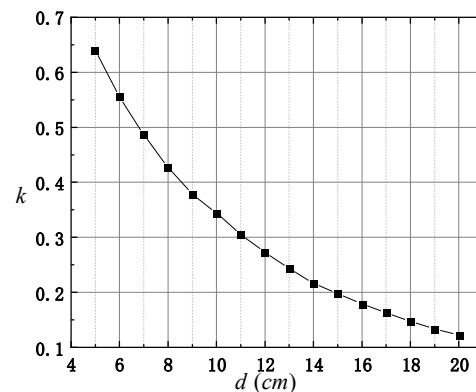


Figure 14. The relationship between k and d .

4.2. Self-Determining Soft-Switching Operation Point

It can be observed from the experiment that there is always a wide soft-switching margin under dynamic coupling coefficient k . Once the duty of S_1 maintains in the soft-switching margin, the IPIFR-WPT system will work in the soft-switching states.

The curves of soft-switching margins with respect to the relative distance d of coils is shown in Figure 15. Notice, at the operation points P_1, P_2 and P_3 , the distances of the coils are 6 cm, 7 cm and 9 cm, respectively, but the duty of S_1 is the same, 20%. And the waveforms working at P_1, P_2 and P_3 are shown in Figure 16.

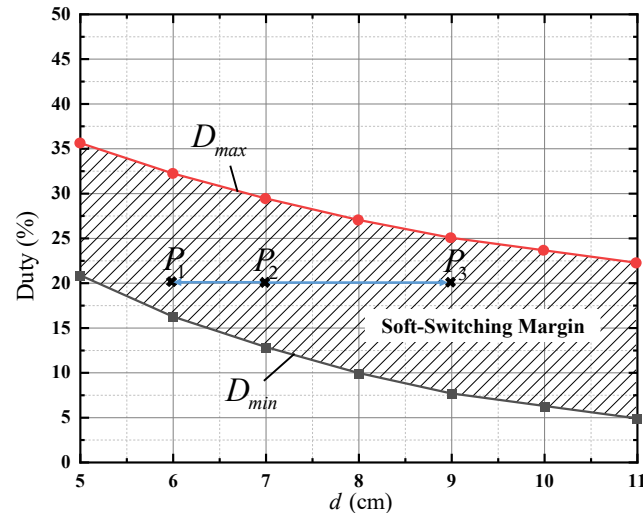


Figure 15. The curves of soft-switching margins with respect to the d .

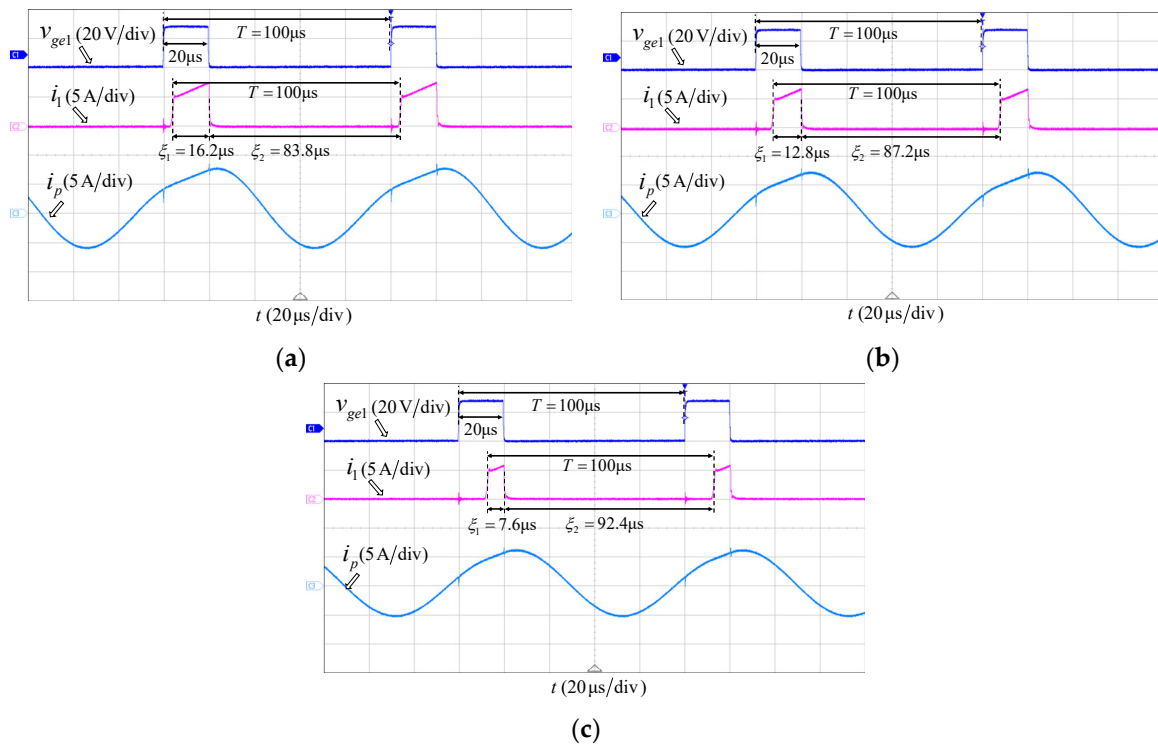


Figure 16. The waveforms under different d and the same duty. (a) $d = 6$ cm, (b) $d = 7$ cm, (c) $d = 9$ cm.

When d equals to (a) 6 cm, (b) 7 cm and (c) 9 cm, respectively, the corresponding waveforms of $v_{gs1}(t), i_l(t)$ and $i_p(t)$ are shown in Figure 16. The determined intervals ξ_1 by the system itself are (a) 16.2 μ s, (b) 12.8 μ s and (c) 7.6 μ s, respectively. Therefore, when the switching strategies remains the same and the relative distance d of coils changes dynamically, the IPIFR-WPT system can keep working in soft-switching states by self-determining its operating point, which operates the same as the theoretical results.

As shown in Figure 17, taking a fixed working cycle $T = 100 \mu\text{s}$, the curves of soft-switching margins with respect to the change in equivalent load resistance R_L are plotted.

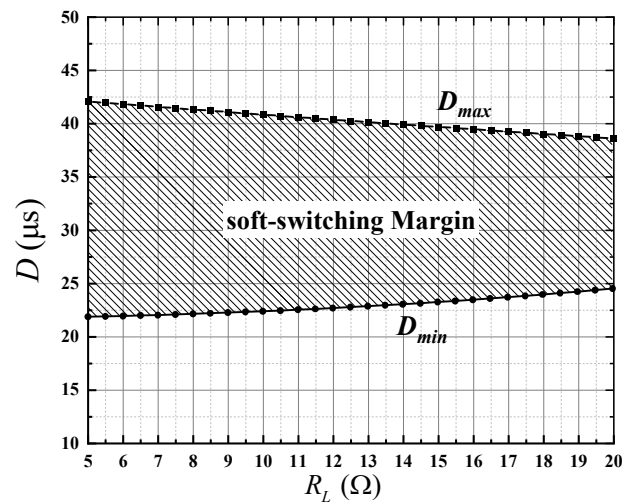


Figure 17. The curves of soft-switching margins with respect to the R_L .

As shown in Figure 17, when the equivalent load resistance R_L increases from 5Ω to 20Ω , although the soft switching range is somewhat narrowed, it can maintain a soft switching margin of nearly 13% or more. And in Figure 17, when the load resistance R_L undergoes dynamic changes within the range of 5Ω to 20Ω , the soft switching duty cycle range of the proposed WPT system still has a large overlap range, which makes the system have an adaptive ability to resist dynamic changes in load resistance R_L .

In Figure 18, the equivalent load resistance R_L is plotted when taking 10Ω , 15Ω , and 20Ω and using the same switching strategy ($D_1 = 25.0 \mu\text{s}$ and $T = 100 \mu\text{s}$). The waveform of the power supply current i_1 and the current i_p on the primary inductor. As shown in Figure 18, regardless of the values of R_L being 10Ω , 15Ω , and 20Ω , the system can meet the boundary conditions under the same switching strategy $\beta_2 (u_p = E_{dc}$ and $i_p > 0)$, meaning that the system can still operate at its respective soft switching operating points, therefore the system can resist dynamic changes in load resistance R_L over a large range.

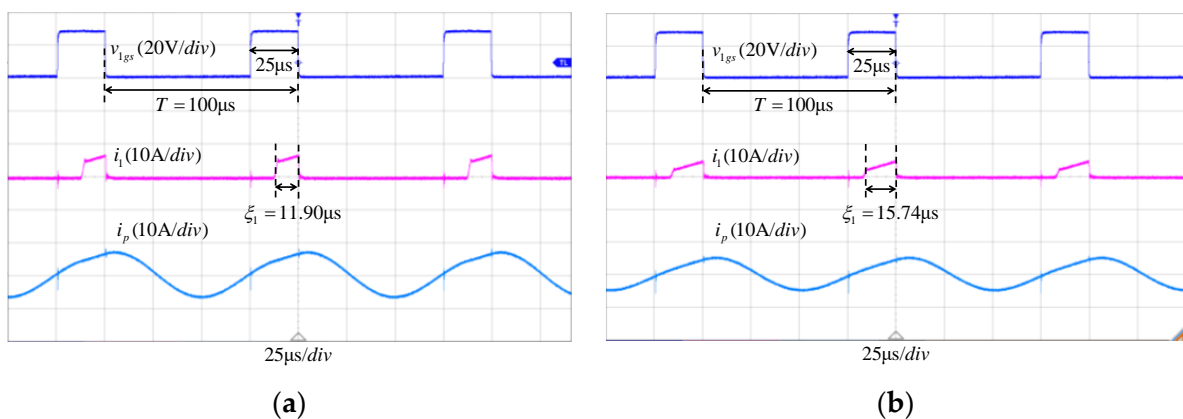


Figure 18. Cont.

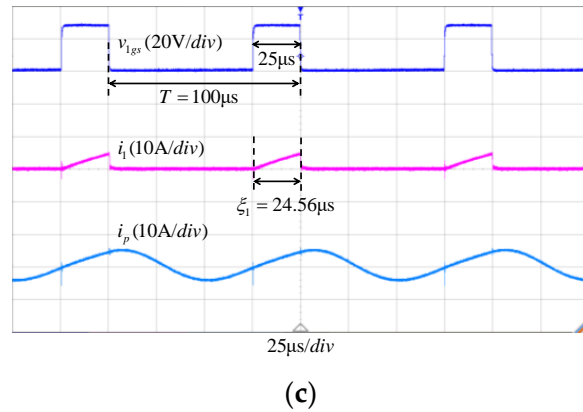


Figure 18. The waveforms under different R_L and the same duty. (a) $R_L = 10 \Omega$, (b) $R_L = 15 \Omega$, (c) $R_L = 20 \Omega$.

4.3. The Monotonicity of Output Power about Cycle

According to the analysis above, the output power shows monotonicity with respect to cycle T . The experimental curves are shown in Figure 19, when the distances d are (a) 6 cm, (b) 8 cm and (c) 10 cm, respectively, the output power increases from (a) 106 W, (b) 54 W, (c) 26 W to (a) 530 W, (b) 537 W, (c) 597 W monotonously with the rise of cycle T from 100 μs to 130 μs , which is pretty close to the calculated results in Figure 11.

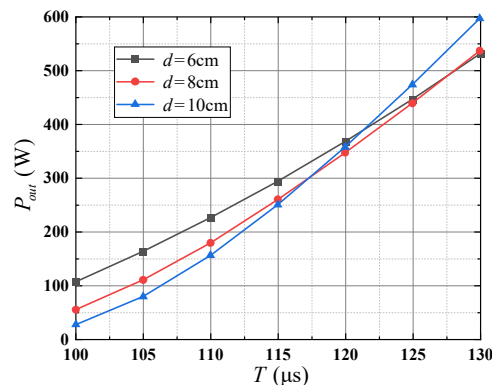


Figure 19. The curves of output power P_{out} with cycle T .

The corresponding efficiencies η are recorded and plotted in Figure 20. The efficiency of the system maintains more than 80% when the coils distance less than 10 cm and achieves 90% under 6 cm coils distance.

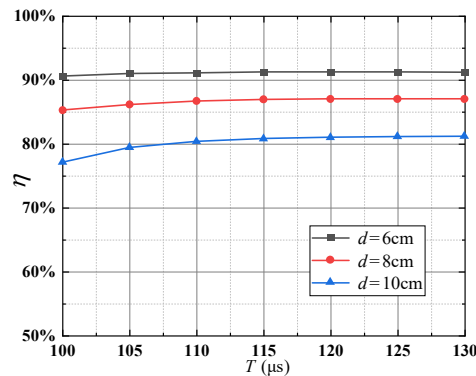


Figure 20. The curves of efficiency η with cycle T .

5. Conclusions

This article presents a double-switch IPIFR-WPT system working in CCM, whose operation modes can be decoupled as two independent processes, the power injection and the free resonance. Different from the fully resonant type of WPT system, the power injection process and the resonance process do not proceed simultaneously. Instead, for the proposed WPT system, the intervals ζ_1 and ζ_2 of the two processes are independent and the power injects into the system only in the time of the interval ζ_1 . It can be known from the theoretical analysis that the operation point of the proposed WPT system is not determined by the switching control strategy, hence there is a wide soft-switching margin to ensure the system operating in soft-switching states. Since the power injected into the system increases monotonously with respect to operation cycle T , thus the output power can be controlled simply by adjusting cycle T . The characteristic of a self-determining soft-switching operation point has been proved in both theory and experiment. Under a fixed switching control strategy, the system maintains soft-switching states without adjusting the switching strategy when the coupling coefficient k rises from 0.4 to 0.6 theoretically or when the relative coils distance d varies from 6 cm to 9 cm experimentally. Hence IPIFR system has a great advantage to resist the dynamic change of coupling coefficient and is more suitable for the reality situation where the environmental factors would cause the movement of coils.

As for the monotonicity of the power curve about cycle T , the output power rises from 106 W to 597 W with the increases of T from 100 μ s to 130 μ s at 10 cm coils distance meanwhile the efficiency almost maintains a constant (80%) and several curves with different coil distances present the monotonicity of output power about the cycle. Hence, the simple method for the IPIFR system to control the output power flexibly is adjusting the operation cycle under a constant coils distance d . Furthermore, if the coupling of the coils becomes stronger, the efficiency of the IPIFR system will rise. Concretely, when the coils distance changes from 10 cm to 6 cm, the average efficiency rises from 80% to 91%.

Author Contributions: Conceptualization, W.W. and D.L.; Methodology, Z.T.; Software, Z.T.; Formal analysis, J.H.; Resources, J.Y.; Writing—original draft, W.W.; Writing—review & editing, W.W. and D.L.; Project administration, W.W. and D.L.; Funding acquisition, J.H. All authors have read and agreed to the published version of the manuscript.

Funding: This research was funded in part by the Natural Science Foundation of China, Grant 52177222, in part by the Natural Science Foundation of Fujian Province, Grant 2021J05262, and in part by the Education Project for Young and Middle aged Teachers of Fujian Provincial Department of Education, Grant JAT200462.

Conflicts of Interest: The authors declare no conflict of interest.

References

1. Zhong, W.; Lee, C.K.; Hui, S.Y. General Analysis on the Use of Tesla's Resonators in Domino Forms for Wireless Power Transfer. *IEEE Trans. Ind. Electron.* **2013**, *60*, 261–270. [[CrossRef](#)]
2. Wu, H.H.; Gilchrist, A.; Sealy, K.D.; Bronson, D. A High Efficiency 5 kW Inductive Charger for EVs Using Dual Side Control. *IEEE Trans. Ind. Inform.* **2012**, *8*, 585–595. [[CrossRef](#)]
3. Zhu, Q.; Zhang, Y.; Liao, C.; Guo, Y.; Wang, L.; Li, F. Experimental Study on Asymmetric Wireless Power Transfer System for Electric Vehicle Considering Ferrous Chassis. *IEEE Trans. Transp. Electrific.* **2017**, *3*, 427–433. [[CrossRef](#)]
4. Zhang, Z.; Zhang, B. Omnidirectional and Efficient Wireless Power Transfer System for Logistic Robots. *IEEE Access* **2020**, *8*, 13683–13693. [[CrossRef](#)]
5. Lu, Y.; Ma, D.B. Wireless Power Transfer System Architectures for Portable or Implantable Applications. *Energies* **2016**, *9*, 1087. [[CrossRef](#)]
6. Feezor, M.D.; Sorrell, F.Y.; Blankinship, P.R. An interface system for autonomous undersea vehicles. *IEEE J. Ocean. Eng.* **2001**, *26*, 522–525. [[CrossRef](#)]
7. Kim, S.; Park, H.; Kim, J.; Kim, J.; Ahn, S. Design and Analysis of a Resonant Reactive Shield for a Wireless Power Electric Vehicle. *IEEE Trans. Microw. Theory Tech.* **2014**, *62*, 1057–1066. [[CrossRef](#)]
8. Yao, Y.; Wang, Y.; Liu, X.; Lin, F.; Xu, D. A Novel Parameter Tuning Method for a Double-Sided LCL Compensated WPT System with Better Comprehensive Performance. *IEEE Trans. Power Electron.* **2018**, *33*, 8525–8536. [[CrossRef](#)]

9. Zhu, Q.; Wang, L.; Guo, Y.; Liao, C.; Li, F. Applying LCC Compensation Network to Dynamic Wireless EV Charging System. *IEEE Trans. Ind. Electron.* **2016**, *63*, 6557–6567. [[CrossRef](#)]
10. Sohn, Y.H.; Choi, B.H.; Lee, E.S.; Lim, G.C.; Cho, G.H.; Rim, C.T. General Unified Analyses of Two-Capacitor Inductive Power Transfer Systems: Equivalence of Current-Source SS and SP Compensations. *IEEE Trans. Power Electron.* **2015**, *30*, 6030–6045. [[CrossRef](#)]
11. Zhou, W.; Ma, H.; He, X. Investigation on Different Compensation Topologies in Inductively Coupled Power Transfer System. *Trans. China Electron. Soc.* **2009**, *24*, 133–139.
12. Han, G.; Liu, Y.; Li, Q.; Xing, Z.; Zhang, Z. A 6.78-MHz distance-insensitive wireless power transfer system with a dual-coupled L-type matching network. *Rev. Sci. Instrum.* **2021**, *92*, 054705. [[CrossRef](#)] [[PubMed](#)]
13. Lim, Y.; Tang, H.; Lim, S.; Park, J. An Adaptive Impedance-Matching Network Based on a Novel Capacitor Matrix for Wireless Power Transfer. *IEEE Trans. Power Electron.* **2014**, *29*, 4403–4413. [[CrossRef](#)]
14. Huang, R.; Zhang, B.; Qiu, D.; Zhang, Y. Frequency Splitting Phenomena of Magnetic Resonant Coupling Wireless Power Transfer. *IEEE Trans. Magn.* **2014**, *50*, 8600204. [[CrossRef](#)]
15. Huang, R.; Zhang, B. Frequency, Impedance Characteristics and HF Converters of Two-Coil and Four-Coil Wireless Power Transfer. *IEEE J. Emerg. Sel. Top. Power Electron.* **2015**, *3*, 177–183. [[CrossRef](#)]
16. Liao, Z.J.; Ma, S.; Feng, Q.K.; Xia, C.; Yu, D. Frequency Splitting Elimination and Utilization in Magnetic Coupling Wireless Power Transfer Systems. *IEEE Trans. Circuits Syst. I Reg. Pap.* **2021**, *68*, 929–939. [[CrossRef](#)]
17. Chen, L.; Hong, J.; Guan, M.; Wu, W.; Chen, W. A Power Converter Decoupled from the Resonant Network for Wireless Inductive Coupling Power Transfer. *Energies* **2019**, *12*, 1192. [[CrossRef](#)]
18. Chen, L.; Hong, J.; Lin, Z.; Luo, D.; Guan, M.; Chen, W. A Converter with Automatic Stage Transition Control for Inductive Power Transfer. *Energies* **2020**, *13*, 5268. [[CrossRef](#)]
19. Chen, L.; Hong, J.; Guan, M.; Lin, Z.; Chen, W. A Converter Based on Independently Inductive Energy Injection and Free Resonance for Wireless Energy Transfer. *Energies* **2019**, *12*, 3467. [[CrossRef](#)]
20. Tang, C.S.; Sun, Y.; Su, Y.G.; Nguang, S.K.; Hu, A.P. Determining Multiple Steady-State ZCS Operating Points of a Switch-Mode Contactless Power Transfer System. *IEEE Trans. Power Electron.* **2009**, *24*, 416–425. [[CrossRef](#)]
21. He, L.; Guo, D. A Clamped and Harmonic Injected Class-E Converter with ZVS and Reduced Voltage Stress Over Wide Range of Distance in WPT System. *IEEE Trans. Power Electron.* **2021**, *36*, 6339–6350. [[CrossRef](#)]

Disclaimer/Publisher’s Note: The statements, opinions and data contained in all publications are solely those of the individual author(s) and contributor(s) and not of MDPI and/or the editor(s). MDPI and/or the editor(s) disclaim responsibility for any injury to people or property resulting from any ideas, methods, instructions or products referred to in the content.